Miyake and Noda *Earth, Planets and Space* (2019) 71:137
https://doi.org/10.1186/s40623-019-1113-8

Earth, Planets and Space

FULL PAPER Open Access

Fully dynamic earthquake sequence simulation of a fault in a viscoelastic medium using a spectral boundary integral equation method: does interseismic stress relaxation promote aseismic transients?

Yuki Miyake[1] and Hiroyuki Noda[2*]

Abstract

Along subduction interfaces or some major faults, a seismogenic layer in the upper crust is underlain by a zone of slow-slip events (SSEs) and tremors, and seismicity disappears at greater depths. The transition between seismogenic and aseismic behavior may be caused by changes in the frictional properties of the fault or changes in viscoelastic properties of the surrounding medium. Although aseismic transients have been numerically generated in previous studies by changing the frictional properties and compared to SSEs, the effect of viscoelasticity on the transition remains to be studied. In this study, we implemented interseismic viscoelastic stress relaxation in a simulation code for two-dimensional antiplane fully dynamic earthquake sequences in a uniform elastic material based on a spectral boundary integral equation method. In the implementation, we developed a suitable algorithm in which the viscoelastic relaxation is calculated by evolution of an "effective slip," which gives viscoelastic stress change on the fault if convolved with a static Green's function. We conducted parametric studies for a fault with a rate-weakening patch on two parameters: viscoelastic relaxation time t_c and characteristic length of the state evolution in the rate- and state-dependent friction law L. The behavior of the simulated fault can be classified into four classes, earthquakes (EQ), aseismic transients (AT), stable sliding (SS), and stuck (ST), in which the central part of the rate-weakening patch has a diminishingly small slip rate and is permanently locked. A phase diagram of the fault behavior shows that there are two different types of seismogenic–aseismic transition. As L increases, an EQ patch changes to an AT patch before becoming an SS patch, as has been reported in previous studies in an elastic limit. The boundary between AT and SS can be explained via linear stability analysis of a system composed of a spring, a dashpot, and sliders. As t_c decreases, the recurrence interval of the earthquakes diverges, and an EQ patch changes to an ST patch unless L is within a narrow range. Therefore, the transition associated with SSEs and tremors is dominated by changes in frictional properties rather than changes in viscoelastic properties.

Keywords: Earthquake sequence simulation, Viscoelasticity, Spectral boundary integral equation method, Memory variable method

Introduction

Since the discovery of slow-slip events (SSEs; Hirose et al. 1999), various types of slow earthquakes have been discovered (e.g., Beroza and Ide 2011) and attracted researchers' interests partly because of their potential relevance to the generation processes of devastating

*Correspondence: noda.hiroyuki.7z@kyoto-u.ac.jp
[2] Research Center for Earthquake Prediction, Disaster Prevention Research Institute, Kyoto University, Gokasho, Uji 6110011, Japan
Full list of author information is available at the end of the article

earthquakes (e.g., Obara and Kato 2016). They are slip phenomena (Hirose et al. 1999; Shelly et al. 2007; Ide et al. 2007) that show different frequency characteristics from ordinal seismic events, and often associated with the seismogenic–aseismic transition. For example, along the Nankai Trough subduction interfaces, a zone of megathrust earthquakes lies between zones of shallower very low-frequency events and deeper long-term SSEs and tremors (Figure 1 in Obara and Kato 2016). On the San Andreas fault, non-volcanic tremors (e.g., Shelly and Hardebeck 2010) and SSEs (Rousset et al. 2019) are observed beneath the seismogenic layer. No significant seismic event is recognized from the even deeper part of the fault. Extensive survey thus far and numerous discoveries of slow earthquakes may have been revealing that it is typical that a seismogenic–aseismic transition is accompanied by slow earthquakes along major faults.

There are several candidate factors responsible for the seismogenic–aseismic transition such as changes in temperature, pressure, fluid pressure, rock type, and so on. Among them, temperature is often considered as a dominant controlling factor (e.g., Chen and Molnar 1983; Hyndman and Wang 1993; Tanaka and Ishikawa 2002). Frictional instability requires rate-weakening friction (Ruina 1983), and the frictional rate-dependency is known to become negative within a restricted range of temperature [e.g., 50–300 °C for granite (Blanpied et al. 1991), 200–300 °C for gabbro (He et al. 2007), and 250–400 °C for pelitic subduction zone material (den Hartog et al. 2013), depending on other experimental conditions]. These temperature ranges are sometimes compared to that of the seismogenic layer (e.g., Scholz 1988). The seismic–aseismic transition numerically reproduced by changing the frictional rate-dependency is associated with repeating aseismic transients near the transition that can be compared to SSEs (e.g., Liu and Rice 2005). A rate-weakening patch produces aseismic transients if it is marginally larger than the critical length of the stability of the steady sliding (e.g., Kato 2003).

Another potentially important effect of temperature is activation of viscoelastic relaxation in the surrounding medium. In the first place, an earthquake releases elastic strain energy and radiates a part of it in the shape of a far-field seismic wave. It is conceivable that efficient relaxation of stress and aseismic release of the strain energy would suppress seismogenesis. Because brittle-plastic transition temperature is different for different rock-forming minerals, lithology may affect the seismogenic depth limit (Magistrale 2002; Hauksson and Meier 2019). Allison and Dunham (2018) simulated a sequence of earthquakes on a strike–slip fault governed by the rate- and state-dependent friction law with depth-variable rate dependency embedded in a power law viscoelastic material. In their simulation with the warmest geothermal gradient in their conditions (30 K/km, their Fig. 7d), a part of the fault within the lower crust and mantle virtually did not slip because of a weaker surrounding medium than the frictional interface. Notably, the simulated fault by Allison and Dunham (2018) is rate-strengthening within the lower crust and thus cannot produce frictional instability there, while the non-volcanic tremor along the San Andreas fault is observed exactly within this depth range (Figure 1 in Veedu and Barbot 2016). It may be important to consider how a rate-weakening patch interacts with the surrounding viscoelastic medium to understand the generation process of slow earthquakes and the nature of the seismogenic–aseismic transition.

As temperature increases with depth, the properties of the frictional interface and the surrounding medium simultaneously change. A question addressed in the present study was which of the two is more important. In laboratory experiments of stick–slip using Maxwell viscoelastic material, changes in the statistics of event size (Yamaguchi et al. 2009) and a decrease in the event magnitude (Namiki et al. 2014) with decreasing loading rate were reported. An experiment with a slower loading rate can be interpreted as a case with a shorter nondimensional relaxation time, and thus can be considered to represent a deeper condition. But the frictional property (e.g., rate-dependency) of the experimentally simulated fault may well change with the loading rate, as reported in many studies of rocks (e.g., Dieterich 1978; Shimamoto 1986; Kawamoto and Shimamoto 1997). Therefore, it is not necessarily clear whether frictional property or viscoelastic relaxation plays the central role in the laboratory observation.

In the present study, we aim to separate these two effects and elucidate the effect of viscoelastic relaxation on the behavior of a rate-weakening patch by conducting numerical simulations of a fault embedded in a uniform Maxwell viscoelastic medium. There are previous studies dealing with more sophisticated geometry and flow law (e.g., Kato 2002; Lambert and Barbot 2016; Zhang and Sagiya 2018; Allison and Dunham 2018). In those studies, inertial effects were only partly incorporated, and simulations were designed to capture large crustal-scale behavior. Our target is the seismogenic–aseismic transition of a rate-weakening patch which may be much smaller than the depth. Inertial effects are essential to study this transition; quasistatic or quasidynamic approximation (Rice 1993) could cause underestimation of maximum slip rate and recurrence interval of the events (Lapusta and Liu 2009). To map out a parametric space, a large number of simulations are required. For a planar fault in an elastic medium, the spectral boundary integral equation method (SBIEM) developed by Lapusta et al. (2000) is one of the

fastest methods for simulation of fully dynamic earthquake sequences. We propose here a new algorithm of the implementation of interseismic viscoelastic relaxation in the elastic simulation using the SBIEM. This implementation does not require significant additional memory or computational cost.

In this paper, "Methodology" section is devoted to an explanation of the methodology. We first briefly review the elastic earthquake sequence simulation using the SBIEM in "The SBIEM for an elastic medium" section and then the newly developed implementation of viscoelastic relaxation is explained in "Implementation of the viscoelastic effect" section. The model setting and design of the parametric study are described in "Model setting" and "Parametric study for relaxation time and frictional properties" sections, respectively. The simulation results are summarized in "Results" section. Based on the results, we discuss whether viscoelastic relaxation promotes aseismic transients or not, in "Does the viscoelastic effect promote aseismic transients?" section. The boundary between steady sliding and repeating aseismic transients in the parametric space is explained via a simple spring–slider–dashpot mode in "Linear stability analysis of a spring–slider–dashpot model" section. The dependency of the fault behavior on the initial condition is discussed in "Dependency on initial conditions" section. Finally, the conclusions of this study are presented in "Conclusions" section.

Methodology

The SBIEM for an elastic medium

The purpose of the present study was to elucidate the seismogenic–aseismic transition of a rate-weakening patch embedded in a viscoelastic medium. To avoid additional complexity, we placed our focus on a geometrically simple two-dimensional antiplane problem with a planar fault embedded in a uniform Maxwell viscoelastic medium. For a planar fault embedded in an elastic medium, the SBIEM developed by Lapusta et al. (2000) is one of the fastest methods that makes use of the Fast Fourier Transformation technique. We implemented the interseismic stress relaxation in this method using a memory variable (e.g., Ruina 1983). In this section, we briefly review the structure of the SBIEM in the elastic case. Then, we explain our implementation of the viscoelastic effect in the following section.

We consider a planer fault with a rate-weakening patch surrounded by a rate-strengthening region (Fig. 1). A Cartesian coordinate system is set such that the fault plane is $y = 0$ and the displacement is in the z-direction. In the antiplane problem, we do not have to consider all components of the displacement vector and the stress tensor

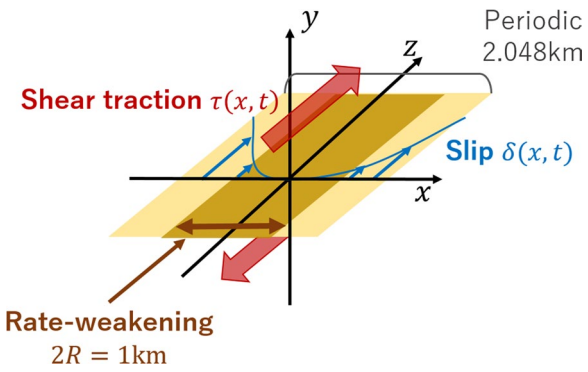

Fig. 1 Antiplane model studied in this study. A planar fault ($y = 0$) is embedded in a Maxwell-viscoelastic material. A rate-weakening patch of a length of $2R = 1$ km (a brown region) is surrounded by a rate-strengthening region (a yellow region), and periodic boundaries are set approximately every $4R$ as indicated by a gray bracket. Slip (blue arrows) and shear traction (red arrows) are in the z-direction

among u_i and σ_{ij}, where i and j are x, y, or z. We abbreviate the components that matter as

$$u(x,y,t) = u_z(x,y,t), \tag{1}$$

$$\sigma_i(x,y,t) = \sigma_{iz}(x,y,t) \quad (i = x,y), \tag{2}$$

where t is time. Note that the variables are independent of z. The slip $\delta(x,t)$, slip rate $V(x,t)$, and shear traction $\tau(x,t)$ on the fault are written as

$$\begin{aligned}\delta(x,t) &= u(x,y=0+,t) - u(x,y=0-,t)\\ &= 2u(x,y=0+,t),\end{aligned} \tag{3}$$

$$V(x,t) = \dot{\delta}(x,t), \tag{4}$$

$$\tau(x,t) = \sigma_y(x,0,t), \tag{5}$$

where the dot represents the partial derivative with respect to t.

In a boundary integral equation method, τ is expressed as (e.g., Lapusta et al. 2000)

$$\tau(x,t) = \tau_0(x,t) + \phi[V](x,t) - \frac{\mu}{2c_s}V(x,t), \tag{6}$$

where τ_0 is the shear traction on the fault without any slip and $\phi[V]$ the convolutional term representing the stress change resulting from the previous fault motion. The last term of Eq. (6) is termed the radiation dumping effect (Rice 1993), which is an instantaneous response between V and τ resulting from acoustic impedance of the S-wave, and explicitly extracted from the convolution. $\phi[V]$ is composed of two terms, the elastostatic stress change ϕ_{st}^{EL} and difference from it ϕ_{dyn},

$$\phi[V] = \phi_{st}^{\mathrm{EL}}[\delta] + \phi_{\mathrm{dyn}}[V]. \tag{7}$$

Note that $\phi_{st}^{\mathrm{EL}}[\delta]$ is a functional of the current slip distribution and $\phi_{\mathrm{dyn}}[V]$ a functional of the spatio-temporal distribution of the previous slip rate. As the contribution of slip rate at a certain previous time to ϕ_{dyn} diminishes as t increases, we can truncate the temporal integral for ϕ_{dyn} and carry on simulations over multiple earthquakes with restricted memory available for storage of history (e.g., Lapusta et al. 2000).

In a spectral method, the functional terms are calculated in the wavenumber domain as

$$\Phi_{\mathrm{dyn}}(k,t) = F\left[\phi_{\mathrm{dyn}}\right] = \int_{t-t_w}^{t} C_D\left(|k|c_s(t-t')\right)\dot{D}(k,t')\,\mathrm{d}t' \tag{8}$$

$$\Phi_{st}^{\mathrm{EL}}(k,t) = F\left[\phi_{st}^{\mathrm{EL}}\right] = -\frac{\mu|k|}{2}D(k,t) \tag{9}$$

where k is the wavenumber in the x-direction, $\mathcal{F}[]$ the Fourier transformation, t_{w} the time window for inertial effects, C_D the integration kernel for the dynamic term, and D and $\dot{D}$ are Fourier transforms of δ and V, respectively. For the expression of C_D, see Lapusta et al. (2000).

An SBIEM for dynamic rupture simulations in a linear viscoelastic medium has been developed by Geubelle (1997). In the problems of our interest, however, the viscoelastic relaxation time t_c of the medium (rock) is much larger than the coseismic timescale. Therefore, we safely ignore the viscoelastic effect in Φ_{dyn} and maintain Eq. (8) unchanged. We modify Eq. (9) to consider interseismic stress relaxation.

Implementation of the viscoelastic effect

In antiplane problems, the constitutive equations of an elastic material and a Maxwell viscoelastic material are represented as

$$\dot{u}_{,i} = \frac{\dot{\sigma}_i}{\mu}, \tag{10}$$

and

$$\dot{u}_{,i} = \frac{1}{\mu}\left(\dot{\sigma}_i + \frac{\sigma_i}{t_c}\right), \tag{11}$$

respectively, where "$,i$" represents the spatial partial derivative in the i-direction and t_c is the relaxation time.

Taking Laplace transformation with respect to time, we obtain for the elastic case

$$\widetilde{u}_{,i} = \frac{1}{\mu}\widetilde{\sigma}_i, \tag{12}$$

and for the viscoelastic case,

$$\widetilde{u}_{,i} = \frac{1}{\mu'}\widetilde{\sigma}_i, \tag{13}$$

where

$$\mu' = \mu\frac{st_c}{st_c+1}. \tag{14}$$

The tildes represent Laplace transformation and s is the Laplace variable. The similarity of Eqs. (12) and (13) is referred to as the correspondence principle of linear viscoelasticity.

The Laplace transformation of Eq. (9) is simply

$$\widetilde{\Phi}_{st}^{\mathrm{EL}}(k,s) = -\frac{\mu|k|}{2}\widetilde{D}(k,s). \tag{15}$$

Owing to the correspondence principle, the viscoelastic version of this term can be written in an analogous form

$$\widetilde{\Phi}_{st}^{\mathrm{VE}}(k,s) = -\frac{\mu'|k|}{2}\widetilde{D}(k,s) = -\frac{\mu|k|}{2}\frac{st_c}{st_c+1}\widetilde{D}(k,s). \tag{16}$$

Taking the inverse Laplace transformation, we obtain the time-domain expression of the viscoelastic quasistatic stress change in a Maxwell material resulting from the previous slip rate as

$$\Phi_{st}^{\mathrm{VE}}(k,t) = -\frac{\mu|k|}{2}\int_0^t \mathrm{e}^{-\frac{(t-t')}{t_c}}\dot{D}\left(k,t'\right)\mathrm{d}t'. \tag{17}$$

This expression involves temporal convolution and we shall not calculate this directly. In the SBIEM, history storage is a limiting factor given the restricted amount of numerical resources. We store the slip rate history within the time window t_{w} to capture inertial effects during earthquakes; additional history storage for interseismic stress relaxation significantly affects the maximum affordable spatial resolution.

Instead of evaluating Eq. (17) by conducting a numerical integral, we reformulate it in a derivative form. If we define a memory variable,

$$D_{\mathrm{eff}}(k,t) = \int_0^t \mathrm{e}^{-\frac{(t-t')}{t_c}}\dot{D}\left(k,t'\right)\mathrm{d}t', \tag{18}$$

then Eq. (17) is written as

$$\Phi_{st}^{\mathrm{VE}}(k,t) = -\frac{\mu|k|}{2}D_{\mathrm{eff}}(k,t). \tag{19}$$

D_{eff} provides the viscoelastic quasistatic stress change in the wavenumber domain if multiplied by the elastic static kernel $-\mu|k|/2$. In this sense, D_{eff} can be termed a Fourier transformation of the effective slip. The time-derivative of Eq. (18) yields

$$\dot{D}_{\mathrm{eff}}(k,t) = \dot{D}(k,t) - \frac{1}{t_c}D_{\mathrm{eff}}(k,t). \tag{20}$$

We would like to point out that the memory variable formulation was used in formulating a rate- and state-dependent friction law by Ruina (1983) when re-formulating an

integral representing decaying memory to a derivative equation of a state variable. We can obtain the integration of Eq. (20) every timestep for a negligible numerical cost; because we calculate $\dot{D}$ in the elastic case, no additional calculation of Fourier transformation is needed. In numerical simulations described in a following section, we explicitly update D^{eff} when updating δ. For more details regarding the numerical algorithm, please see Noda and Lapusta (2010).

Model setting

Figure 1 shows the model setting investigated in this study. A planar fault is embedded in a Maxwell viscoelastic infinite medium with the shear wave speed $c_s = 3000$ m/s, the shear modulus $\mu = 30$ GPa, and the viscoelastic relaxation time t_c which varies in a parametric study. We place a rate-weakening patch of width $2R$ using a smoothed boxcar function (e.g., Noda and Lapusta 2010) and set periodic boundaries every $4.096R$ (1024 grid points) in the x-direction. The origin is at the center of the rate-weakening patch

Our selection of scales of speed and stress is typical for rocks. However, selection of the length scale requires more consideration. We investigate a simple model and consider an infinite medium. This means that R must be much smaller than the depth of the patch in natural conditions for the analysis to be applicable. For a larger patch, our analysis may be applicable only qualitatively or additional physics may come into play. Along the San Andreas fault, non-volcanic tremors occur within a depth range about 20–30 km (Shelly and Hardebeck 2010). Then, we select a length scale $2R = 1$ km for a presentational purpose. Notably, the system can be scaled in length and time by multiplying the same factor while maintaining the scale of speed and stress. If our analysis is to be applied to a smaller patch of $2R = 100$ m, then one must multiply a factor of 0.1 to the physical properties of the dimensions of length and time, such as the length scale in the friction law, viscoelastic relaxation time t_c, and recurrence interval of the event t_{rec}.

For the friction law, we adopt the arcsinh-regularized rate-and-state friction (RSF) law (Rice et al. 2001) with the aging law for the state evolution

$$\tau = \sigma f = \sigma a(x) \sinh^{-1}\left[\frac{V(x,t)}{2V_{\mathrm{pl}}} \exp\left(\frac{f_0 + b(x)\ln\left(V_{\mathrm{pl}}\theta(x,t)/L\right)}{a(x)}\right)\right] \tag{21}$$

$$\frac{\partial\theta}{\partial t} = 1 - \frac{V(x,t)\theta(x,t)}{L} \tag{22}$$

where f is the friction coefficient, θ is the state variable, σ is the normal stress on the fault, a and b are nondimensional parameters representing the amount of direct and evolution effects, respectively, L is the state evolution slip distance, and f_0 is the reference friction coefficient at a reference slip rate V_{pl}. We use $\sigma = 100$ MPa, $f_0 = 0.6$, and $V_{\mathrm{pl}} = 10^{-9}$ m/s, and vary L in a parametric study. The distributions of a and b are shown in Fig. 2. In the rate-weakening patch, $a/b = 0.8$.

Inertial effects are not important as long as V is small, but are significant when V is large. The radiation damping effect becomes comparable to the direct effect in the rate- and state-dependent friction law when $V \approx V_{\mathrm{dyn}} = 2c_s a\sigma/\mu = 0.4$ m/s; thus, it significantly affects the solution at a slightly smaller V than V_{dyn}. We define earthquakes by a threshold value in the slip rate at 0.1 m/s.

The system is driven by far-field loading $\tau_0 = 60$ MPa so that there is a uniform steady-state solution at $V = V_{\mathrm{pl}}$. The numerical experiment in this study is designed to investigate how stability of the steady-state solution changes as the viscoelastic relaxation becomes efficient.

It must be noted that short relaxation time t_c would cause low stress level on a fault in natural situation, and thus decreasing t_c with keeping τ_0 may not be realistic. For a smaller value of τ_0, a uniform steady-state solution at much smaller slip rate $V_{\mathrm{pl}}' \ll V_{\mathrm{pl}}$ exists if f_0 is appropriately distributed in such a way that τ_0 corresponds with steady-state frictional resistance at V_{pl}'. The qualitative behavior of such a system including changes in the stability is essentially the same in a quasistatic limit, although the timescale changes.

We add initial perturbation to the state variable θ as

$$\ln\left(V_{\mathrm{pl}}\theta(x,0)/L\right) = \ln\left(V_{\mathrm{pl}}/V_{\mathrm{ini}}\right)\left(1 + \frac{0.01x}{2R}\right), \tag{23}$$

where $V_{\mathrm{ini}} = 0.999V_{\mathrm{pl}}$ unless otherwise noted. In addition to uniform perturbation, we set a small gradient to break the symmetry under the initial condition.

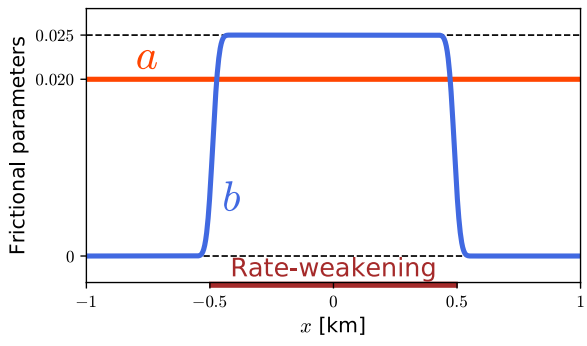

Fig. 2 Spatial variation in frictional parameters a and b in the rate- and state-dependent friction (RSF) law. a is uniform and b is given by a smoothed boxcar function (e.g., Noda and Lapusta 2010). In the central part of the rate-weakening patch, $a/b = 0.8$

Parametric study for relaxation time and frictional properties

To observe the effect of viscoelastic stress relaxation on the behavior of a rate-weakening patch of various brittleness, we conducted parametric studies on two parameters: state-evolution slip distance L and viscoelastic relaxation time t_c.

Let us introduce nondimensional representation of the two parameters to examine the system behavior independent of its length scale. For a fault governed by the aging law in an elastic medium, nucleation size R_c^{EL} is given by (Rubin and Ampuero 2005)

$$R_c^{\mathrm{EL}} = \frac{1}{\pi}\left(\frac{b}{b-a}\right)^2 \frac{\mu L}{b\sigma} \tag{24}$$

for a relatively large a/b in earthquake sequence simulations (e.g., Noda and Hori 2014). A rate-weakening patch in an elastic medium produces repeating seismic events if $R_c^{\mathrm{EL}} \ll R$, aseismic transients if $R_c^{\mathrm{EL}} \sim R$, and steady sliding if $R_c^{\mathrm{EL}} \ll R$ (Kato 2003; Liu and Rice 2007; Chen and Lapusta 2009). In a following section, we present the results of the parametric study as a function of R_c^{EL}/R, which is proportional to L. Notably, the nucleation size (Eq. 24) is in the case with an elastic medium, and viscoelasticity may affect the nucleation size.

The viscoelastic relaxation time t_c is nondimensionalized by a characteristic time scale of loading to the rate-weakening patch t_{load}, which we define as

$$t_{\mathrm{load}} = 2\frac{a\sigma R}{\mu V_{\mathrm{pl}}}. \tag{25}$$

This is a timescale during which loading to the patch due to creep motion outside becomes significant with respect to the frictional direct effect. With $2R = 1$ km, $t_{\mathrm{load}} = 6.67 \times 10^7$ s.

The parametric study was conducted on the two nondimensional parameters R_c^{EL}/R and t_c/t_{load} by changing L and t_c. In the two-dimensional parametric study, we examine R_c^{EL}/R from 0.172 to 1.91 and t_c/t_{load} from 0.946 to 2.37. The rectangular area in the parametric space is divided by a 50×50 mesh and we ran 2500 earthquake sequence simulations at the grid points. In addition, we ran a series of elastic simulations for reference which correspond to $t_c/t_{\mathrm{load}} = \infty$. In each simulation used to map out the two-dimensional parametric space, we calculated the fault behavior until the 10th earthquake or $t = 200$ years ($= 94.6 t_{\mathrm{load}}$).

Results

Elastic case for reference

Here, we show the system behavior of the elastic cases for reference. The range of ν investigated captures the seismogenic–aseismic transition. With a relatively small value of R_c^{EL}/R, the rate-weakening patch produces repeating earthquakes as shown in Fig. 3a. Note that the horizontal discontinuities shown in Fig. 3a represent earthquakes and nucleation occurs in a creeping part of the rate-weakening patch. A case is classified as "EQ" if the maximum slip rate in the latter half of the simulation exceeds 0.1 m/s. As R_c^{EL}/R increases, the maximum slip rate decreases. Even if it becomes smaller than 0.1 m/s, and thus inertial effects are not important compared with the frictional direct effect, transient slip events repeatedly occur (Fig. 3b). A case is classified as "AT" if the small initial perturbation grows and if the case is not classified as EQ. With an even larger value of R_c^{EL}/R, a steady-state solution becomes linearly stable (Fig. 3c). A case is classified as "SS" if the initial perturbation decays toward the steady sliding. As mentioned before, this type of transition has been reported in many previous studies.

Based on these simulations, we define the recurrence interval t_{rec} and the maximum slip rate V_{max} in the following manner. We output a timeseries of the spatially maximum value of V in each simulation. Then, we obtained at most ten local maxima in the time series corresponding to earthquakes and defined t_{rec} as the average of the intervals between them if there were more than three earthquakes. Although a spin-up period is included, we the standard deviation of the intervals is no more than 0.1% of t_{rec}. V_{max} is defined as the maximum value of V during the latter one-half of the simulations to avoid the effect of initial perturbation.

Viscoelastic effects on earthquake sequence

Transition without aseismic transients

Figure 4 shows a typical example of the seismogenic–aseismic transition resulting from a decrease in t_c/t_{load} while maintaining R_c^{EL}/R constant at 0.4. Figure 4a shows

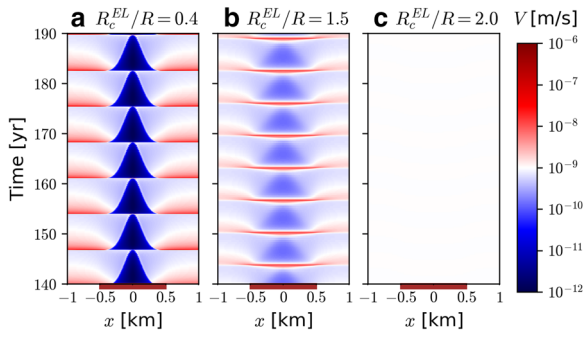

Fig. 3 Spatiotemporal distribution of V in elastic cases with different R_c^{EL}/R values. **a** $R_c^{\mathrm{EL}}/R = 0.4$. The system produces repeating earthquakes approximately every 7.15 years ($= 3.38 t_{\mathrm{load}}$). **b** $R_c^{\mathrm{EL}}/R = 1.5$. V_{max} is smaller than 0.1 m/s. Repeating AT occur around the patch. **c** $R_c^{\mathrm{EL}}/R = 1.5$. Variation in V cannot be recognized in the color scale adopted. The steady-state solution is stable

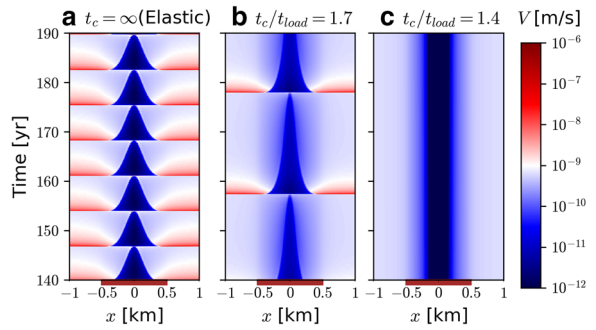

Fig. 4 Spatiotemporal distribution of V in viscoelastic cases with different t_c/t_{load} values. **a** An elastic limit, identical to the case plotted in Fig. 3a. The system produces repeating earthquakes every approximately 7.15 years ($= 3.38t_{\mathrm{load}}$). **b** $t_c/t_{\mathrm{load}} = 1.7$. t_c is approximately one-half of t_{rec} in the elastic limit. Earthquakes repeat at a longer interval of 20.6 years ($= 9.74t_{\mathrm{load}}$) than in the elastic case. **c** $t_c/t_{\mathrm{load}} = 1.4$. The central part of the rate-weakening patch is locked and no earthquake occurs during simulation

an elastic case ($t_c = \infty$), which is identical to the case plotted in Fig. 3a. This case is EQ, and the recurrence interval t_{rec} is 7.15 years ($= 3.38t_{\mathrm{load}}$). With decreasing t_c, the recurrence interval increases (Fig. 4b). Interseismic propagation of creep fronts into the rate-weakening patch is slower than that in the elastic case such that it takes longer for the creeping part of the fault to host nucleation of an earthquake. As t_c further decreases, the recurrence interval becomes longer than the simulated time (Fig. 4c). In such cases, the slip rate at the center of the rate-weakening patch diminishes with time following a power law. The rate-weakening patch seems to be stuck. A case is classified as "ST" if the region of very small slip rate ($V < 10^{-11}$ m/s) is increasing at the end of the simulation.

Figure 5 shows the recurrence interval t_{rec} as a function of t_c/t_{load} with $R_c^{\mathrm{EL}}/R = 0.35$. The increase in t_{rec} as t_c decreases can be fit very well by a function

$$t_{\mathrm{rec}} = \frac{\alpha}{t_c/t_{\mathrm{load}} - \widetilde{t}_{\mathrm{cr}}} + \beta, \tag{26}$$

where α, β, and $\widetilde{t}_{\mathrm{cr}}$ are fitting parameters, as recognized by a slope of -1 in a log–log plot (Fig. 5b). Here, $\widetilde{t}_{\mathrm{cr}}$ is a critical nondimensional relaxation time. In the case plotted in Fig. 5, we obtained the optimum parameters such $\alpha = (26.3 \pm 0.1)$ year, $\beta = (72.8 \pm 0.4)$ year, and $\widetilde{t}_{\mathrm{cr}} = 1.5182 \pm 0.0002$. If $t_c/t_{\mathrm{load}} \leq \widetilde{t}_{\mathrm{cr}}$, we expect that no earthquake would occur, however, long we might simulate; the rate-weakening patch is permanently stuck. There is no range of t_c for AT along this line in the parametric space.

Two-dimensional parametric study

Distribution of V_{max} in the parametric space of $\left(t_c/t_{\mathrm{load}}, R_c^{\mathrm{EL}}/R\right)$ is shown in Fig. 6, as well as the boundaries between the four behavioral classes: EQ, AT, SS, and ST. An EQ patch produces repeating earthquakes during which V_{max} is greater than 0.1 m/s and inertial effects become important. With increasing R_c^{EL}/R, V_{max} sharply decreases from approximately V_{dyn}, but sustained oscillation occurs while $R_c^{\mathrm{EL}}/R \approx 1$. This is the region for AT. With further increasing R_c^{EL}/R, the amplitude of the sustained oscillation decreases, and the patch finally produces decaying oscillation

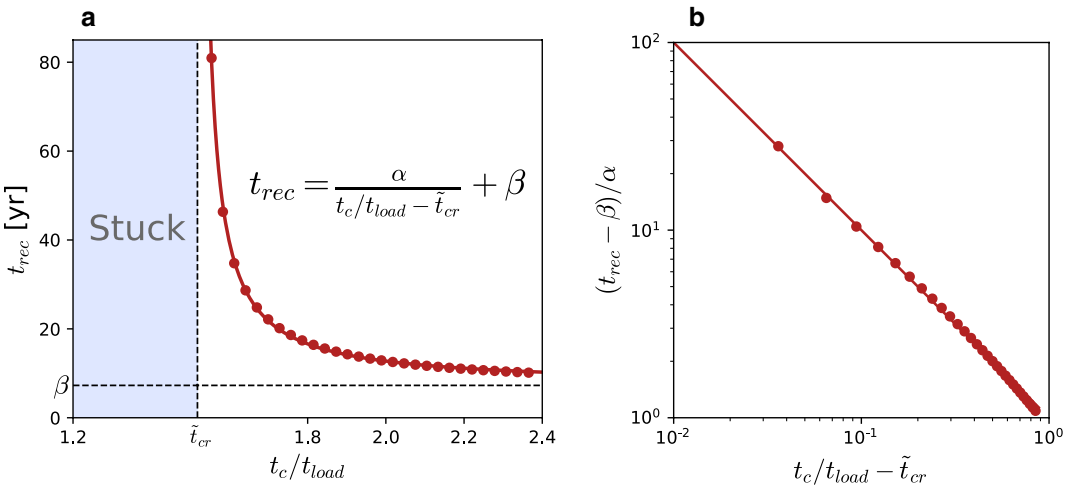

Fig. 5 Change in the recurrence interval due to viscoelastic relaxation. **a** Plot of the recurrence interval of earthquakes t_{rec} as a function of t_c/t_{load} with $R_c^{\mathrm{EL}}/R = 0.35$. A solid line represents the best-fit model to the simulation results which diverges at $\widetilde{t}_{\mathrm{cr}}$. **b** A log–log plot of **a**, showing a power law decay with a slope of −1

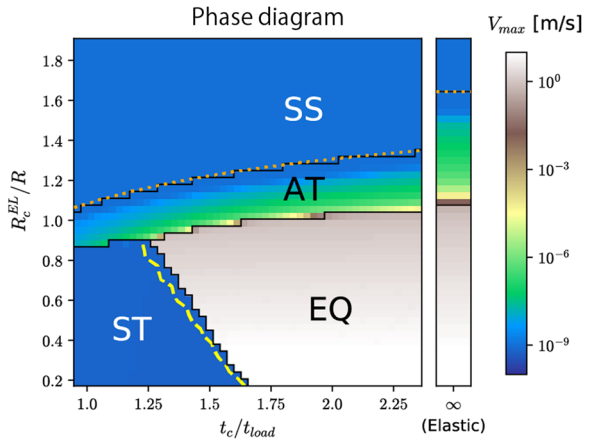

Fig. 6 Phase diagram of the fault behavior and V_{max} as a function of t_c/t_{load} and R_c^{EL}/R. *EQ* earthquakes, *AT* aseismic transients, *SS* steady slip, *ST* stuck. The boundaries of these behaviors are indicated by black lines. The initial slip rate in the rate-weakening patch is $V_{ini} = 0.999V_{pl}$. The yellow dashed line represents the critical relaxation time $\widetilde{t}_{cr}$ estimated from the divergence of t_{rec} (Fig. 5). The orange dotted line indicates a theoretical boundary between SS and AT derived via a linear stability analysis described in "Linear stability analysis of a spring–slider–dashpot model" section. Elastic cases ($t_c = \infty$) are shown in a right thin panel

toward SS. These three behavioral types have already been reported in the previous studies (e.g., Kato 2003; Liu and Rice 2007; Chen and Lapusta 2009) in elastic cases. Here, we have confirmed that they also exist in viscoelastic cases. In addition, we discovered that the rate-weakening patch becomes permanently stuck (ST) when t_c decreases from the EQ regime unless R_c^{EL}/R is within a rather narrow range greater than 0.9.

There are two types of seismogenic–aseismic transitions. One is the transition from EQ to SS via AT. This is the case for both elastic and viscoelastic cases with increasing L and can be realized by decreasing t_c if R_c^{EL}/R is carefully selected near 1. The other type of transition is from EQ to ST without associated AT. In this transition, the recurrence interval of the earthquakes increases and diverges at a critical value of t_c, as demonstrated in the previous section.

The yellow dashed line shown in Fig. 6 represents the nondimensional critical relaxation time $\widetilde{t}_{cr}$ estimated for each value of R_c^{EL}/R. $\widetilde{t}_{cr}$ seems to depend nearly linearly on R_c^{EL}/R and the line is cut by the boundary of an AT regime.

Discussion

Does the viscoelastic effect promote aseismic transients?

In the phase diagram, the seismogenic limit of the nondimensional relaxation time $\widetilde{t}_{cr}$ is of the order of 1. The corresponding dimensional relaxation time is $t_c \approx 10^8$ s for $2R = 1$ km. A typical value for the viscosity of the lower crust is approximately 10^{19} Pa s (e.g., Thatcher et al. 1980) and $\mu = 30$ GPa leads to $t_c \approx 3 \times 10^8$ s. Nonlinear rheology may contribute to shorten the effective relaxation time for transient deformation. Therefore, the simulated range of t_c may be relevant to natural conditions and thus we believe that viscoelastic relaxation may play an important role in seismogenic–aseismic transition. For a smaller rate-weakening patch, t_{load} is smaller and thus t_c/t_{load} is larger if t_c is fixed. Viscoelastic relaxation is less important for a smaller patch. Therefore, the viscoelastic effect may affect statistics of the size of earthquakes near the seismogenic–aseismic transition by reducing the number of large earthquakes (Yamaguchi et al. 2009; Namiki et al. 2014). It may not, however, promote generation of AT.

As shown in Fig. 6, we found two types of seismogenic–aseismic transitions. With increasing L, the transition from EQ to SS via AT occurs, similar to elastic cases. With decreasing t_c, however, the transition from EQ to ST occurs without AT unless R_c^{EL}/R is fine-tuned near 1. Because an earthquake rupture typically shows significantly smaller early-stage rupture than the final size of the earthquake (e.g., Uchide and Ide 2010), the R_c^{EL}/R of natural seismogenic patches cannot be near 1. Then, the change in t_c alone cannot explain the transition associated with AT. Changes in frictional properties seem to be required to generate aseismic transients near the transition.

The higher and lower limits of R_c^{EL}/R of the regime of AT both decrease as t_c decreases, with their difference decreasing. Thus, a range of L for AT eventually narrows as the viscoelastic stress relaxation becomes efficient. In this sense, the viscoelastic effect suppresses generation of aseismic transients.

Linear stability analysis of a spring–slider–dashpot model

To explain the boundary between AT and SS as shown in Fig. 6, we conducted a linear stability analysis of a simplified spring–slider–dashpot model as shown in Fig. 7. Two sliders of the same area represent the rate-weakening patch and surrounding rate-strengthening part of the fault. They are connected by a Maxwell spring–dashpot element with stiffness k (stress/length) and relaxation time t_c which support stress of ξ. The system is driven by far-field loading τ_0 subjected to both sliders. Then, the shear stress supported by the two sliders can be written as

$$\tau_1 = \tau_0 + \xi, \quad \tau_2 = \tau_0 - \xi. \tag{27}$$

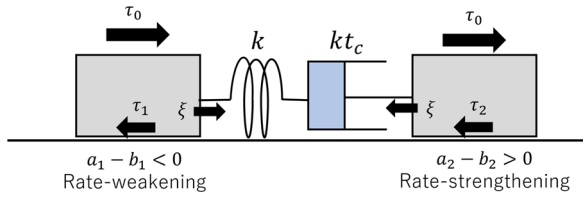

Fig. 7 Schematic diagram of the investigated spring–slider–dashpot model. Two blocks representing rate-weakening and rate-strengthening patches are connected by a Maxwell element composed of a spring of stiffness k and a dashpot of viscosity kt_c

For simplicity, we use a logarithmic rate- and state-dependent friction law in the aging law formulation (Dieterich 1979; Ruina 1983)

$$\tau_i = \sigma f_0 + \sigma a_i \log\left(\frac{V_i}{V_{\rm pl}}\right) + \sigma b_i \log\left(\frac{\theta_i V_{\rm pl}}{L}\right), \tag{28}$$

$$\frac{{\rm d}\theta_i}{{\rm d}t} = 1 - \frac{V_i \theta_i}{L}, \tag{29}$$

where $i = 1$ for the rate-weakening slider and $i = 2$ is for the rate-strengthening slider. The frictional properties are taken consistently with the continuum model, $a_1 = a_2 = 0.02$, $b_1 = 0.025$, and $b_2 = 0$ (see Fig. 2); thus, we have only one state variable $\theta = \theta_1$. By solving Eqs. (27) and (28) for V_i, we can obtain expressions of $V_1(\xi, \theta_1)$ and $V_2(\xi)$.

The change in ξ due to the deformation of the spring and the dashpot is

$$\frac{{\rm d}\xi}{{\rm d}t} = k(V_2 - V_1) - \frac{\xi}{t_c}. \tag{30}$$

Then, we can obtain the time-derivative of a two-dimensional variable (ξ, θ_1) as

$$\frac{\rm d}{{\rm d}t}\begin{pmatrix}\xi \\ \theta_1\end{pmatrix} = \begin{pmatrix} k(V_2(\xi) - V_1(\xi,\theta_1)) - \frac{\xi}{t_c} \\ 1 - \frac{V_1(\xi,\theta_1)\theta_1}{L}\end{pmatrix}. \tag{31}$$

At the steady state, $\xi = 0$, $\theta_1 = L/V_{\rm pl}$, and $V_1 = V_2 = V_{\rm pl}$. By linearizing Eq. (31) around it, and searching for a condition under which the real part of the eigenvalues of the Jacobian matrix becomes zero (Hopf bifurcation), we obtained a critical stiffness for linear stability as

$$k_{\rm crit} = \frac{\sigma a_2}{L(a_1+a_2)}\left\{(b_1 - a_1) - \frac{La_1}{V_{\rm pl} t_c}\right\}. \tag{32}$$

This is consistent with the well-known expression of the critical stiffness for a spring–slider model $\sigma(b_1 - a_1)/L$ (Ruina 1983) at a limit of both a_2 and $t_c \to \infty$. Note that block #2 steadily slides at the limit of $a_2 \to \infty$, providing a constant load-point velocity to block #1.

To compare this simplified model to the continuum model we simulated, we introduce a geometrical factor γ such that $k = \gamma\mu/2R$. Then, the critical condition $k = k_{\rm crit}$ yields the critical value of the state evolution slip distance $L_{\rm crit}$ as a function of t_c, by solving (32) for L

$$L_{\rm crit}(t_c) = \left(1 + \frac{a_2\gamma^{-1}}{a_1+a_2}\frac{t_{\rm load}}{t_c}\right)^{-1} L_{\rm crit}^{\rm EL} \tag{33}$$

where

$$L_{\rm crit}^{\rm EL} = \frac{(b_1-a_1)}{(a_1+a_2)}\frac{\sigma a_2}{\gamma\mu}2R. \tag{34}$$

To evaluate the geometrical factor γ, we estimate $L_{\rm crit}^{\rm EL}$ from the boundary between AT and SS in the elastic case which separates the decaying oscillation and asymptotically growing oscillation at the end of simulations. We obtained $L_{\rm crit}^{\rm EL} = 0.086$ m which corresponds to $R_c^{\rm EL}/R = 1.64$ and thus $\gamma = 0.97$. This estimation of γ close to 1 may imply the plausibility of the simplified model.

Substituting $L_{\rm crit}(t_c)$ for L in Eq. (24), we can predict the linear stability boundary in the two-dimensional parametric space as

$$\left(R_c^{\rm EL}/R\right)_{\rm crit} = 1.64\left(1 + \frac{a_2\gamma^{-1}}{a_1+a_2}\frac{t_{\rm load}}{t_c}\right)^{-1}. \tag{35}$$

This is indicated by an orange dashed line in Fig. 6 and consistent with the boundary between SS and AT.

Dependency on initial conditions

In drawing the phase diagram (Fig. 6), we used a small initial perturbation to the steady-state solution. We found that the amplitude of the perturbation matters. Figure 8 shows three simulation results with $R_c^{\rm EL}/R = 1$

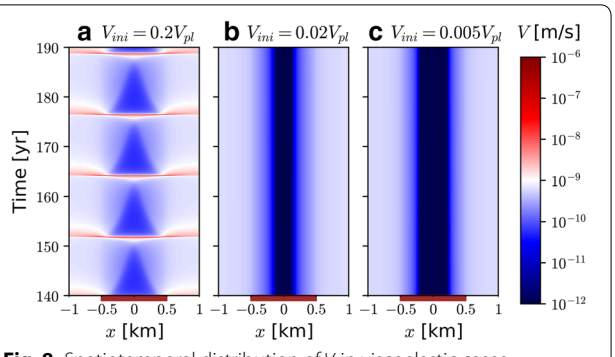

Fig. 8 Spatiotemporal distribution of V in viscoelastic cases with different $V_{\rm ini}$ values and with $R_c^{\rm EL}/R = 1$ and $t_c/t_{\rm load} = 1.5$. **a** $V_{\rm ini} = 0.2V_{\rm pl}$. The system produces repeating AT, similar to the case with small initial perturbation (Fig. 6). **b** $V_{\rm ini} = 0.02V_{\rm pl}$. The rate-weakening patch is stuck. **c** $V_{\rm ini} = 0.005V_{\rm pl}$. The rate-weakening patch is stuck similar to **b**, but the stuck part of the patch is larger

and $t_c/t_{\rm load} = 1.5$ under different initial conditions, $V_{\rm ini} = 0.2V_{\rm pl}$, $0.02V_{\rm pl}$, and $0.005V_{\rm pl}$ (Eq. 23) from left to right. At $V_{\rm ini} = 0.2V_{\rm pl}$ (Fig. 8a), the initial perturbation is sufficiently small that the system falls to the same limit cycle (AT) as that of $V_{\rm ini} = 0.999V_{\rm pl}$. At $V_{\rm ini} = 0.02V_{\rm pl}$ (Fig. 8b), however, the central part of the rate-weakening patch becomes permanently stuck. With an even smaller value of $V_{\rm ini}$, the stuck part of the rate-weakening patch is larger (Fig. 8c).

The trajectories of (V, τ) at $x = 0$ in these three cases are plotted in Fig. 9. Immediately after beginning of the simulations, τ increases because $V_{\rm ini}$ is smaller than the slip rate outside the patch $V_{\rm pl}$. If the trajectory crosses the frictional steady-state dependency $\tau = \sigma f_{\rm ss}(V)$ (dashed line in Fig. 9), then the state variable θ decreases and the trajectory can extend in the right-bottom direction in Fig. 9. The efficient stress relaxation weakens the elastic loading to the rate-weakening patch. If the trajectory fails to reach $\tau = \sigma f_{\rm ss}(V)$, θ has to keep increasing and the trajectory tends to extend to the left (deceleration). The semi-horizontal part of the trajectories in the permanently stuck cases is similar to a horizontal trajectory in a creep test for a rate-weakening slider (Dieterich 1981).

Figure 10 shows a distribution of $V_{\rm max}$ similar to that of Fig. 6, but with a different initial condition $V_{\rm ini} = 0.56V_{\rm pl}$. The same phase boundaries as in Fig. 6 are shown for comparison in black. The yellow dashed line in Fig. 10 is $\widetilde{t}_{\rm cr}$ estimated by Eq. (26) for the cases with $V_{\rm ini} = 0.56V_{\rm pl}$ and agrees well with that plotted in Fig. 6. Large initial perturbation [i.e., long distance between the initial point and the uniform steady-state solution in the phase space (Fig. 9)] expands the region for ST. In earthquake sequence simulations in an elastic medium, the system typically spins up to a limit cycle and selection of initial conditions is not very important. Our result implies that selection of initial conditions may matter in dealing with a viscoelastic system.

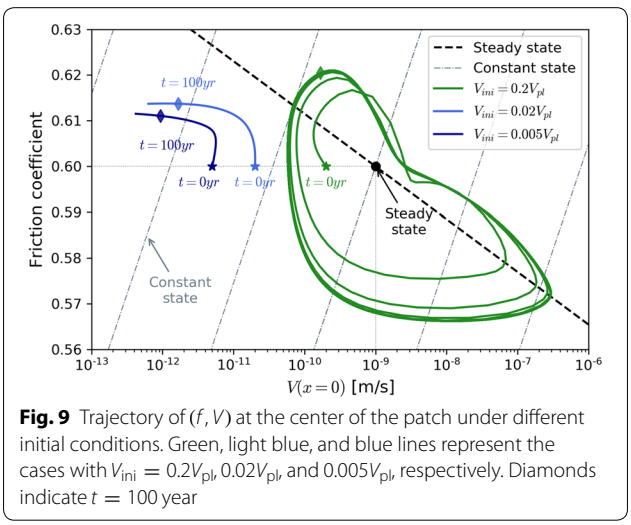

Fig. 9 Trajectory of (f, V) at the center of the patch under different initial conditions. Green, light blue, and blue lines represent the cases with $V_{\rm ini} = 0.2V_{\rm pl}$, $0.02V_{\rm pl}$, and $0.005V_{\rm pl}$, respectively. Diamonds indicate $t = 100$ year

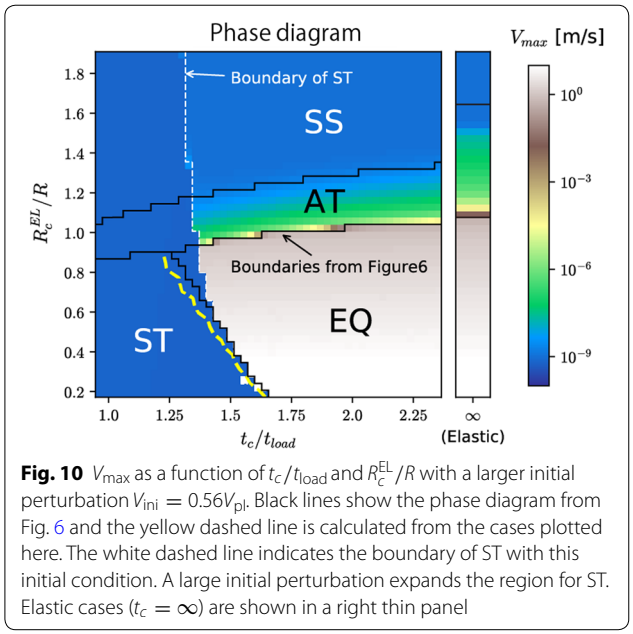

Fig. 10 $V_{\rm max}$ as a function of $t_c/t_{\rm load}$ and $R_c^{\rm EL}/R$ with a larger initial perturbation $V_{\rm ini} = 0.56V_{\rm pl}$. Black lines show the phase diagram from Fig. 6 and the yellow dashed line is calculated from the cases plotted here. The white dashed line indicates the boundary of ST with this initial condition. A large initial perturbation expands the region for ST. Elastic cases ($t_c = \infty$) are shown in a right thin panel

Conclusions

We implemented interseismic viscoelastic stress relaxation to a dynamic earthquake sequence simulation with a spectral boundary integral equation method by developing a new memory variable formulation in the wavenumber domain. Although the method is restricted to geometrically simple problems, the additional computational cost is negligible such that the code is suitable for mass simulations in parametric studies of simple problems.

To investigate whether the seismogenic–aseismic transition accompanied by SSEs is caused by a change in the frictional property or off-fault material properties, we conducted a parametric study of two parameters: relaxation time t_c and frictional state-evolution slip distance L. We discovered that there were two different types of seismogenic–aseismic transitions. One is the transition from EQ to SS via generation of aseismic transients AT. This mainly occurs because of the change in the frictional property. The other is from EQ to ST associated with divergence of the recurrence interval, which is caused by a decrease in t_c unless L is within a narrow range. The EQ–SS transition is accompanied by AT, while AT is absent in the EQ–ST transition. Therefore, it is difficult to explain the generation of SSEs by the decrease in t_c. The boundary between AT and SS was quantitatively explained by a linear stability analysis using a spring–slider–dashpot model. The

range of L for AT decreases with decreasing t_c, which suggests that viscoelastic relaxation suppresses generation of AT. We also found that for the viscoelastic case the simulated fault behavior depends on the initial perturbation added to the system. A large perturbation results in the rate-weakening patch being stuck even though a stable attractor (SS or AT) exists.

Acknowledgements
We thank members of Research Center of Earthquake Prediction, Kyoto University for meaningful discussions.

Authors' contributions
HN developed the new algorithm and designed the problem setting. YM coded the new method and carried out the parameter study. Both authors contributed in interpretation of the results, discussions, and composing the manuscript. Both authors read and approved the final manuscript.

Funding
This study is supported by MEXT KAKENHI Grant Number 26109007, JSPS KAKENHI Grant Number 19K04038, and by the Ministry of Education, Culture, Sports, Science and Technology (MEXT) of Japan, under its Earthquake and Volcano Hazards Observation and Research Program.

Availability of data and materials
We do not use any observation data in the present study. Simulation code is given by Nadia Lapusta in Caltech, and the authors do not have a right to make it open to public.

Ethics approval and consent to participate
Not applicable.

Consent for publication
Not applicable.

Competing interests
The authors declare that they have no competing interests.

Author details
[1] beBit, Incorporated, 4-2-1 Kudan-kita, Chiyoda ward, Tokyo 1020073, Japan. [2] Research Center for Earthquake Prediction, Disaster Prevention Research Institute, Kyoto University, Gokasho, Uji 6110011, Japan.

Received: 12 July 2019 Accepted: 23 November 2019
Published online: 05 December 2019

References

Allison KL, Dunham EM (2018) Earthquake cycle simulations with rate-and-state friction and power-law viscoelasticity. Tectonophysics 733:232–256. https://doi.org/10.1016/j.tecto.2017.10.021
Beroza GC, Ide S (2011) Slow earthquakes and nonvolcanic tremor. Annu Rev Earth Planet Sci 39:271–296. https://doi.org/10.1146/annurev-earth-040809-152531
Blanpied ML, Lockner DA, Byerlee JD (1991) Fault stability inferred from granite sliding experiments at hydrothermal conditions. Geophys Res Lett 18:609–612. https://doi.org/10.1029/91GL00469
Chen T, Lapusta N (2009) Scaling of small repeating earthquakes explained by interaction of seismic and aseismic slip in a rate and state fault model. J Geophys Res 114:B01311. https://doi.org/10.1029/2008JB005749
Chen W-P, Molnar P (1983) Focal depths of intracontinental and intraplate earthquakes and their implications for the thermal and mechanical properties of the lithosphere. J Geophys Res 88:4183–4214
den Hartog SAM, Niemeijer AR, Spiers CJ (2013) Friction on subduction megathrust faults: beyond the illite–muscovite transition. Earth Planet Sci Lett 373:8–19. https://doi.org/10.1016/j.epsl.2013.04.036
Dieterich JH (1978) Time-dependent friction and the mechanics of stick–slip. Pure Appl Geophys 116:790–806. https://doi.org/10.1029/JB084iB05p02161
Dieterich JH (1979) Modeling of rock friction 1. Experimental results and constitutive equations. J Geophys Res 84:2161–2168
Dieterich JH (1981) Constitutive properties of faults with simulated gouge. In: Carter NL et al (eds) Geophysical monograph series, vol 24. AGU, Washington, D. C., pp 103–120
Geubelle PH (1997) A numerical method for elastic and viscoelastic dynamic fracture problems in homogeneous and biomaterial systems. Comput Mech 20:20–25
Hauksson E, Meier M-A (2019) Applying depth distribution of seismicity to determine thermo-mechanical properties of the seismogenic crust in Southern California: comparing lithotectonic blocks. Pure Appl Geophys 176:1061–1081. https://doi.org/10.1007/s00024-018-1981
He C, Wang Z, Yao W (2007) Frictional sliding of gabbro gouge under hydrothermal conditions. Tectonophysics 445:353–362. https://doi.org/10.1016/j.tecto.2007.09.008
Hirose H, Hirahara K, Kimata F, Fujii N, Miyazaki S (1999) A slow thrust slip event following the two 1996 Hyuganada Earthquakes beneath the Bungo Channel, Southwest Japan. Geophys Res Lett 26:3237–3240. https://doi.org/10.1029/1999GL010999
Hyndman RD, Wang K (1993) Thermal constraints on the zone of major thrust earthquake failure: the Cascadia subduction zone. J Geophys Res 98:2039–2060
Ide S, Shelly DR, Beroza GC (2007) Mechanism of deep low frequency earthquakes: further evidence that deep non-volcanic tremor is generated by shear slip on the plate interface. Geophys Res Lett 34:L03308. https://doi.org/10.1029/2006GL028890
Kato N (2002) Seismic cycle on a strike–slip fault with rate- and state-dependent strength in an elastic layer overlying a viscoelastic half-space. Earth Planets Space 54:1077–1083. https://doi.org/10.1186/BF03353305
Kato N (2003) Repeating slip events at a circular asperity: numerical simulation with a rate- and state-dependent friction law. Bull Earthq Res Inst 78:151–166
Kawamoto E, Shimamoto T (1997) Mechanical behavior of halite and calcite shear zones from brittle to fully-plastic deformation and a revised fault model. In: Zheng Y, et al (eds) Structural geology & geomechanics: proceedings of the 30th international geological congress, vol 14, pp 89–105
Lambert V, Barbot S (2016) Contribution of viscoelastic flow in earthquake cycles within the lithosphere–asthenosphere system. Geophy Res Lett 43:10142–10154. https://doi.org/10.1002/2016gl070345
Lapusta N, Liu Y (2009) Three-dimensional boundary integral modeling of spontaneous earthquake sequences and aseismic slip. J Geophys Res 114:1–25. https://doi.org/10.1029/2008JB005934
Lapusta N, Rice JR, Ben-Zion Y, Zheng G (2000) Elastodynamic analysis for slow tectonic loading with spontaneous rupture episodes on faults with rate- and state-dependent friction. J Geophys Res 105:23765–23789. https://doi.org/10.1029/2000jb900250
Liu Y, Rice JR (2005) Aseismic slip transients emerge spontaneously in three-dimensional rate and state modeling of subduction earthquake sequences. J Geophys Res 110:1–14. https://doi.org/10.1029/2004JB003424
Liu Y, Rice JR (2007) Spontaneous and triggered aseismic deformation transients in a subduction fault model. J Geophys Res 112:1–23. https://doi.org/10.1029/2007JB004930
Magistrale H (2002) Relative contributions of crustal temperature and composition to controlling the depth of earthquakes in Southern California. Geophys Res Lett 29:1447. https://doi.org/10.1029/2001GL014375
Namiki A, Yamaguchi T, Sumita I, Suzuki T, Ide S (2014) Earthquake model experiments in a viscoelastic fluid: a scaling of decreasing magnitudes of earthquakes with depth. J Geophys Res 119:3169–3181. https://doi.org/10.1002/2014JB011135
Noda H, Hori T (2014) Under what circumstances does a seismogenic patch produce aseismic transients in the later interseismic period? Geophys Res Lett 41:7477–7484. https://doi.org/10.1002/2014GL061676
Noda H, Lapusta N (2010) Three-dimensional earthquake sequence simulations with evolving temperature and pore pressure due to shear heating: effect of heterogeneous hydraulic diffusivity. J Geophys Res 115:B12314. https://doi.org/10.1029/2010JB007780

Obara K, Kato A (2016) Connecting slow earthquakes to huge earthquakes. Science 353:253–258. https://doi.org/10.1126/science.aaf1512
Rice JR (1993) Spatio-temporal complexity of slip on a fault. J Geophys Res 98:9885–9997. https://doi.org/10.1029/93JB00191
Rice JR, Lapusta N, Ranjith K (2001) Rate and state dependent friction and the stability of sliding between elastically deformable solids. J Mech Phys Solids 49:1865–1898. https://doi.org/10.1016/S0022-5096(01)00042-4
Rousset B, Bürgmann R, Campillo M (2019) Slow slip events in the roots of the San Andreas fault. Sci Adv 5:eaav3274. https://doi.org/10.1126/sciadv.aav3274
Rubin AM, Ampuero J-P (2005) Earthquake nucleation on (Aging) rate and state faults. J Geophys Res 110:1–24. https://doi.org/10.1029/2005JB003686
Ruina AL (1983) Slip instability and state variable friction laws. J Geophys Res 88:10359–10370. https://doi.org/10.1029/jb088ib12p10359
Scholz CH (1988) The brittle-plastic transition and the depth of seismic faulting. Geol Rundsch 77:319–328. https://doi.org/10.1007/BF01848693
Shelly DR, Hardebeck JL (2010) Precise tremor source locations and amplitude variations along the lower-crustal central San Andreas fault. Geophys Res Lett 37:1–5. https://doi.org/10.1029/2010GL043672
Shelly DR, Beroza GC, Ide S (2007) Non-volcanic tremor and low-frequency earthquake swarms. Nature 446:305–307. https://doi.org/10.1038/nature05666
Shimamoto T (1986) Transition between frictional slip and ductile flow for halite shear zones at room temperature. Science 231:711–714
Tanaka A, Ishikawa Y (2002) Temperature distribution and focal depth in the crust of the northeastern Japan. Earth Planets Space 54:1109–1113. https://doi.org/10.1186/BF03353310
Thatcher W, Matsuda T, Kato T, Rundle JB (1980) Lithospheric loading by the 1896 Riku-u Earthquake, Northern Japan: implications for plate flexure and asthenospheric rheology. J Geophys Res 85:6429–6435
Uchide T, Ide S (2010) Scaling of earthquake rupture growth in the Parkfield area: self-similar growth and suppression by the finite seismogenic layer. J Geophys Res 115:B11302. https://doi.org/10.1029/2009jb007122
Veedu DM, Barbot S (2016) The Parkfield tremors reveal slow and fast ruptures on the same asperity. Nature 532:361–365. https://doi.org/10.1038/nature17190
Yamaguchi T, Ohmata S, Daoi M (2009) Regular to chaotic transition of stick–slip motion in sliding friction of an adhesive gel-sheet. J Phys Condens Matter 21:205105. https://doi.org/10.1088/0953-8984/21/20/205105
Zhang X, Sagiya T (2018) Intraplate strike–slip faulting, stress accumulation, and shear localization of a crust–upper mantle system with nonlinear viscoelastic material. J Geophys Res Solid Earth 123:9269–9285. https://doi.org/10.1029/2018jb016421

Publisher's Note